Article
JOURNAL OF UNIVERSITY OF BABYLON
For Pure and Applied Sciences (JUBPAS)
Vol. 34 ; No. 2| 2026

Study the Effect of Table Salt Concentration in Water on the Absorptivity of Gamma Rays Emitted from the Radioactive Source Cs-137.

Ali F. Marmoss

Babylon, Governorate Directorate of Education

E-mail address alimarmoos25@gmail.com

دراسة تأثير ملح الطعام في الماء على إمتصاصية أشعة كاما المنبعثة من المصدر المشعCs-137

Accepted: 16/6/2026 **Published:** 30/6/2026

ABSTRACT

This research investigated the influence of table salt concentration in water on the absorption of gamma rays emitted from a cesium-137 (Cs-137) radioactive source. The measurements were performed using the Universal Computer Spectrometer (UCS-30), which represents the latest generation of nuclear spectroscopy systems developed by Spectrum Techniques LLC, following earlier versions such as UCS-20.

The experimental results demonstrated that the gross area and net area of the gamma-ray energy spectrum decrease progressively with increasing salt concentration in a fixed volume of water (200 ml). In contrast, the photopeak centroid, full width at half maximum (FWHM), and energy resolution were found to increase as the salt concentration increased. These findings indicate that the absorptivity of water for gamma radiation is enhanced by the addition of salt, leading to reduced photon counts and degraded spectral resolution.

The study highlights the significant role of solution density in modifying gamma-ray attenuation and detector response, providing useful insights for applications in radiation shielding, environmental monitoring, and nuclear physics experiments.

Keywords: Cs-137 Gamma-ray absorption, NaI(Tl) scintillation detector , Salt concentration in water, Energy resolution (FWHM).

ISSN: 2312-8135 | Print ISSN: 1992-0652
info@journalofbabylon.com | jub@itnet.uobabylon.edu.iq | www.journalofbabylon.com
مجلة جامعة بابل للعلوم الصرفة والتطبيقية مجلة جامعة بابل للعلوم الصرفة والتطبيقية

ISSN: 2312-8135 | Print ISSN: 1992-0652

info@journalofbabylon.com | jub@itnet.uobabylon.edu.iq | www.journalofbabylon.com

INTRODUCTION

The use of radioactive elements has become one of the most powerful and versatile tools in modern scientific research, spanning the fields of physics, environmental science, and biology. The decay of radioactive nuclei produces various types of radiation that are emitted isotopically from the source. As these radiations travel initially in straight paths, they undergo interactions with atoms in the medium, leading to scattering, absorption, and attenuation. The extent of these interactions depends on both the type and energy of the radiation as well as the physical and chemical properties of the material through which it passes [1]– [3].

The detection of nuclear radiation has advanced significantly with the development of nuclear physics. Radiation detectors are designed to register and measure the energy of emitted particles or photons, and their operation is fundamentally based on the interaction between radiation and the detector material. Charged particles can be detected directly, while neutral particles such as neutrons are detected indirectly through their interactions with matter that produce secondary charged particles [4].

Different types of detectors are optimized for different purposes, as no single detector can fulfill all requirements simultaneously. For example, some detectors provide high energy resolution but at the expense of detection efficiency. Despite these differences, all detectors share the common function of collecting information from radiation–matter interactions, though the mechanisms of information collection vary. In gas and semiconductor detectors, charges are released and collected on electrodes, while in scintillation detectors, photons are produced and subsequently converted into electronic pulses using photomultipliers. Thus, the method of information collection depends strongly on the detector type [5].

Fluorescence detectors, particularly those based on iodide crystals (Z = 53), are widely used due to their high absorptivity and broad applications in nuclear radiation detection, health physics, and related fields. These detectors are often surrounded by materials of varying thickness and composition, which serve as shielding against background radiation in low-intensity experiments or to reduce interference from laboratory equipment such as power supplies and support structures. However, these surrounding materials can themselves act as secondary sources of radiation, thereby influencing the measured spectrum [6]– [8].

The scintillation detector, which is central to this study, operates on the principle that gamma-ray interactions with the detector crystal produce flashes of light, or scintillations. These light flashes are then converted into electronic signals by a photomultiplier tube, enabling the detection and analysis of gamma radiation [9].

MATERIALS AND METHODS

1.Introduction

The system is based on a thallium-activated sodium iodide [NaI(Tl)] scintillation detector, and each of its components was carefully arranged to achieve the most accurate results. Figure (1) illustrates the major parts of the system, which include the scintillation crystal coupled with the photomultiplier tube, the preamplifier, the high-voltage supply, the main amplifier, the multichannel analyzer, and the computer interface. In addition to describing the configuration of

ISSN: 2312-8135 | Print ISSN: 1992-0652
info@journalofbabylon.com | jub@itnet.uobabylon.edu.iq | www.journalofbabylon.com

the system, this chapter also explains the spectral regions of interest and the standard radioactive sources used in the measurements.

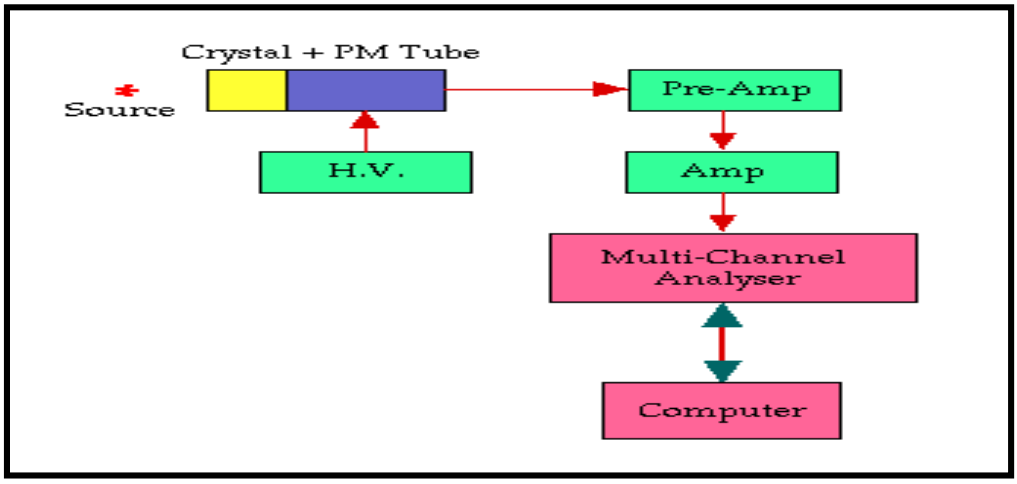

Figure (1): Parts of the electronic counting and analysis system.

2. Measurement system:

The gamma-ray spectrum of the Cs-137 source was measured at a fixed distance of 1 cm between the source and the detector. The measurements were carried out using the UCS-30 system (Spectrum Techniques LLC), which is widely used in nuclear radiation detection. The detector employed was a NaI(Tl) scintillation crystal with dimensions of 1.5 × 1 inches and a density of 3.67 g/cm³. Each spectrum was recorded with an integration time of 100 seconds. Figure (2) presents the main components of the electronic system used in the experiment.

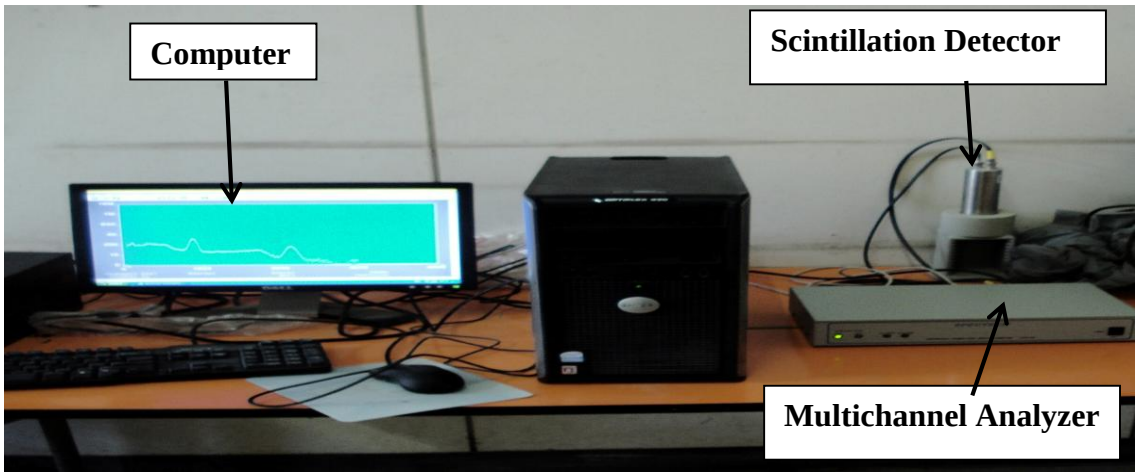

Figure (2): Represents the electronic setup applied in this study.

2.1 Scintillation Detector

The scintillation detector consists of two primary elements: the scintillator crystal and the photomultiplier tube. The NaI(Tl) crystal emits scintillation photons when it absorbs gamma radiation, as the de-excitation of the crystal material releases light [10] , [11]. These photons strike the photocathode of the photomultiplier tube, where they liberate electrons. The electrons are then multiplied through successive dynodes, producing a cascade of secondary electrons. The

ISSN: 2312-8135 | Print ISSN: 1992-0652
info@journalofbabylon.com | jub@itnet.uobabylon.edu.iq | www.journalofbabylon.com

resulting amplified pulse, collected at the anode, serves as a direct indicator of the ionizing radiation that interacted with the crystal [12]. Figure (3) illustrates the electron multiplication process within the dynodes.

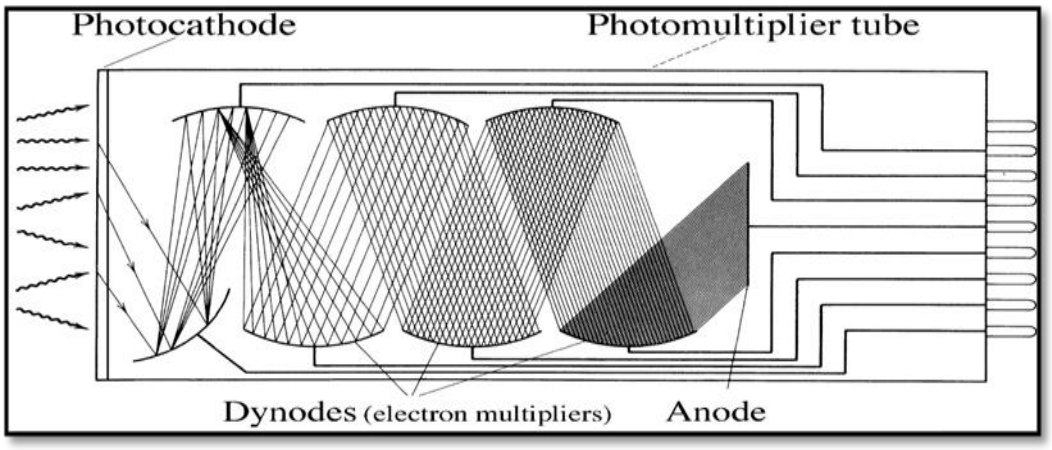

Figure (3): Electron multiplication during dynodes [12].

2.2 .High Voltage Power Supply:

The photomultiplier tube requires a stable high-voltage supply to operate effectively. In this study, a power supply with a range of 0–2000 volts was used. The voltage was delivered through a divider network to ensure proper biasing of the dynodes.

2.3 Photomultiplier Base and Preamplifier Base :

The photomultiplier base distributes the high voltage evenly across the dynodes, ensuring uniform electron multiplication. The preamplifier, located close to the detector, receives the weak charge pulses generated by the scintillation crystal and converts them into current pulses, which are then transformed into voltage pulses. These signals are amplified to a level suitable for further processing by the main amplifier, without distortion of their amplitude.

In addition to amplification, the preamplifier performs pulse shaping, which is essential for distinguishing true radiation signals from electronic noise. Proper shaping reduces noise, improves the definition of the pulse, and enhances the pulse-to-noise ratio, thereby improving the detector's energy resolution [14] , [15].

The preamplifier also ensures impedance matching between the detector and the subsequent electronic circuitry, particularly the main amplifier. This prevents signal loss and distortion. Because the pulses generated by the detector are extremely weak, the preamplifier is mounted very close to the detector to minimize attenuation during transmission through connecting wires[16].

2.4. Main Amplifier:

The main amplifier further amplifies the shaped pulses from the preamplifier to a level that can be accurately measured and analyzed by the multichannel analyzer (MCA). It improves the signal-to-noise ratio, filters out unwanted noise, and ensures that the output pulse amplitude is

ISSN: 2312-8135 | Print ISSN: 1992-0652 | www.journalofbabylon.com | jub@itnet.uobabylon.edu.iq | info@journalofbabylon.com

directly proportional to the input pulse amplitude. This proportionality, known as gain, is critical for accurate spectral analysis. The main amplifier is integrated within the MCA system [17].

2.5. Multichannel Analyzer :

The multichannel spectrum analyzer(MCA) is an advanced device designed for gamma-ray spectroscopy. Its primary advantage lies in its ability to analyze large numbers of pulses with high precision. The MCA performs three main functions: pulse amplitude analysis, multichannel sorting, and data storage. It processes the amplified pulses, records them, and displays the resulting gamma-ray spectrum as a visual output. The MCA integrates a main amplifier and can be configured to operate with different channel capacities (256, 512, 1024, 2048, or 4096), depending on the resolution required [18].

3. Radioactive source:

The radioactive source used in this study was cesium-137 (Cs-137), prepared in a disc-shaped form with a diameter of 2.5 cm. Table (1) summarizes its main properties, including activity, half-life, and gamma-ray energy.

Table (1) Radioactive source used in the research.

Radioactivity Source	Activity (μCi)	Half-Life	Energy (MeV)
Cs-137	0.9121	30.2 Years	0.662

The radioactive efficiency (A) is calculated from the following equation. [19]

$$A = A_{\circ}\, e^{-\lambda T_d} \qquad \ldots\ldots\ldots\ldots (10)$$

where $A_{\circ}$ is the efficiency of the radioactive source at the time of manufacture. T_d is the delay time.

λ is the decay constant and is given by the following equation. [20]

$$\lambda = \ln 2 / T_{1/2} \qquad \ldots\ldots\ldots\ldots\ldots (11)$$

where $T_{1/2}$ is the half-life of the radioactive source.

4. Gamma ray spectrum:

The NaI(Tl) scintillation detector produces an energy spectrum that contains peaks and continuous distributions depending on the type of photon interaction. Each interaction contributes to the appearance of one or more peaks, depending on the photon energy. Figure (4) shows a typical Cs-137 spectrum, illustrating the main spectral regions [21].

ISSN: 2312-8135 | Print ISSN: 1992-0652
info@journalofbabylon.com | jub@itnet.uobabylon.edu.iq | www.journalofbabylon.com

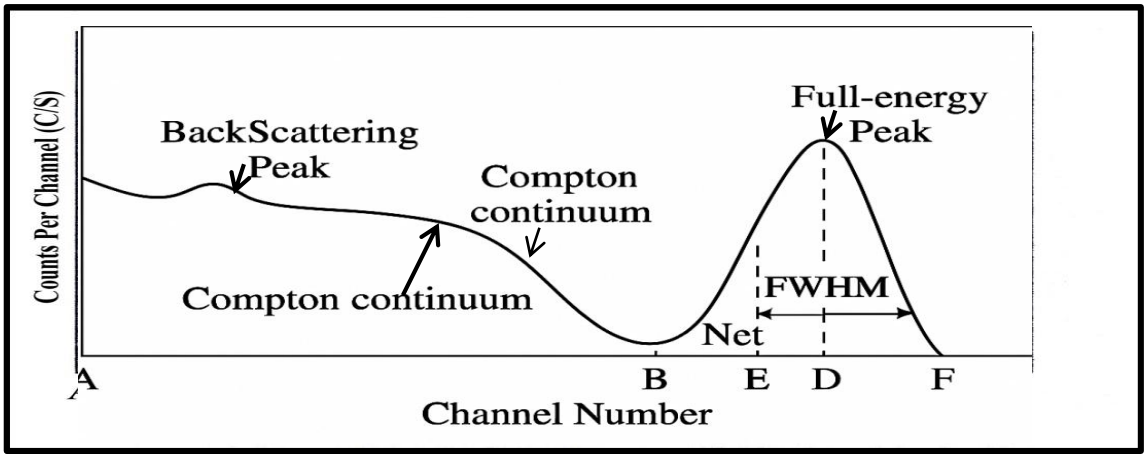

Figure (4): Typical spectrum illustrating the energy spectrum regions of gamma rays using a cesium source Cs-137.[21]

4.1 X-Ray Escape Peak:

This peak generally appears in gamma-ray spectra at low energies and is caused by the interaction of photons with the material surrounding the detector.

4.2 Back Scattering Peak:

The Backscattering Peak is a spectral feature that appears in nearly all gamma-ray spectra. It originates from the scattering of incident photons at an angle of 180° relative to their original direction, caused by interactions with electrons in the material that either coats the radioactive source or surrounds the detector. This process results in photons being redirected back toward the detector, producing a distinct peak in the spectrum. The backscattering peak is particularly prominent in scintillation detectors, where the encapsulating material of the scintillation crystal contributes significantly to this effect. The presence of this peak provides important information about the scattering environment and the materials surrounding the detector, as it reflects the degree of photon polarization and the interaction cross-section of the surrounding medium [21].

4.3 Continuous Compton Distribution:

The Continuous Compton Distribution represents the broad, continuous portion of the gamma-ray spectrum that precedes the location of the photo peak and extends up to the Compton edge (E_c), which corresponds to the maximum energy transferred to a recoil electron during Compton scattering. This distribution arises because gamma photons undergo partial energy transfer to electrons in the detector material, producing a wide range of recoil electron energies. The Compton continuum also extends below the photo peak due to secondary absorption of scattered photons.

Furthermore, Compton scattering occurring in the materials surrounding the detector contributes additional distortions to the spectrum. The magnitude of this contribution depends on several factors: the energy of the incident photon, the scattering angle, and the atomic number of the material responsible for the scattering. As a result, the Compton continuum is an unavoidable

ISSN: 2312-8135 | Print ISSN: 1992-0652

info@journalofbabylon.com | jub@itnet.uobabylon.edu.iq | www.journalofbabylon.com

component of gamma-ray spectra, and its analysis is essential for understanding the interaction processes and for distinguishing the true photo peak from background contributions [21].

4.4. Photo Peak:

The Photopeak corresponds to the complete absorption of the energy of a gamma-ray photon within the scintillation crystal of the detector. This feature arises from the photoelectric effect, in which the entire photon energy is transferred to an electron in the detector material. The photopeak is the most significant region of the gamma-ray spectrum because it provides the most accurate representation of the incident photon energy.

The position of the photopeak (its centroid) and its width are critical parameters for energy calibration and resolution. These parameters vary directly with the photon energy, as well as with instrumental factors such as applied high voltage, amplifier gain, and the number of channels in the multichannel analyzer. Because of its central role in energy determination, the photopeak is used as the primary reference for most calculations in gamma spectroscopy. Accurate identification and measurement of the photopeak are therefore essential for evaluating the performance of the detector and for conducting precise nuclear radiation analyses [22].

4.5 Escaping Peaks that follow the production of the pair:

Escaping Peaks These peaks appear in gamma-ray spectra with energy greater than 1.02MeV. When the pair is generated and annihilated and the two annihilation photons are generated and absorbed into the detector, a peak will appear at energy E_γ (incident photon energy), or a peak will appear at energy (E_γ - 0. 511) MeV, when one photon escapes from the detector and is called the single escape peak, or a peak appears at (E_γ - 1.02) MeV when both photons escape from the detector and is called the double escape peak[22].

5. Energy Resolution:

Energy Resolution is the ability of the detector to distinguish particles or photons with different and converging energies, and the performance of any detector used to measure energy is represented by the width of the pulse distribution of the single-energy source, and the width is measured at the middle of the peak and is called Full Width at Half Maximum (FWHM) and the energy resolvability in analyzers is given by the following relationship [23]. As in Figure (5).

$$\mathbf{E.R} = \frac{\mathbf{FWHM}}{\mathbf{C}} \times \mathbf{100}\ \% \qquad \text{.....(12)}$$

where **C** is the location of the optical peak.

ISSN: 2312-8135 | Print ISSN: 1992-0652
info@journalofbabylon.com | jub@itnet.uobabylon.edu.iq | www.journalofbabylon.com

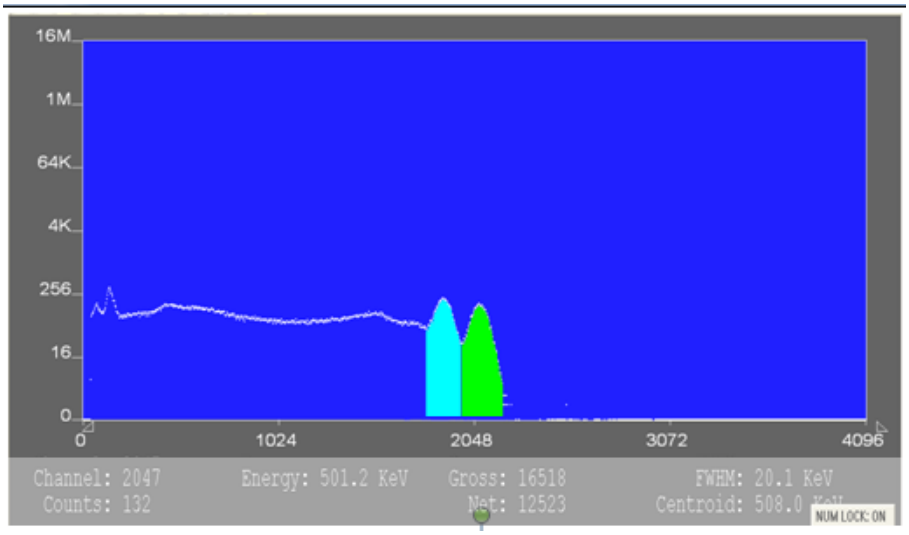

Figure (5): shows the energy spectrum of Cs-137.

Good energy resolution is possible when the spectrum contains two closely spaced energy peaks. If E1 and E2 are the values of the two closely spaced energies, then when $\{E_2-E_1 > 2(FWHM)\}$, the detector can distinguish between the two energies. When $\{E_2-E_1 = 2(FWHM)\}$, the two peaks appear separate but only partially. When $\{E_2-E_1 \geq 2(FWHM)\}$, the two peaks merge into a single peak equal to the sum of the two peaks [13] .

RESULTS AND DISCUSSION

1. Introduction

This section presents in detail the calculations and experimental results obtained during the measurements performed with the NaI(Tl) scintillation detector in conjunction with the Cs-137 radioactive source. The analysis focuses on the influence of varying amounts of table salt dissolved in 200 ml of pure water on the absorption of gamma rays, and how this affects the spectral parameters such as gross and net areas, peak width, centroid position, and energy resolution.

2. Studying the region of Gamma radiation spectrum

The gamma-ray spectrum regions were carefully examined using a Cs-137 source positioned at a fixed distance of 1 cm from the detector. The measurements and subsequent calculations are summarized in Table (2).

To evaluate the effect of increasing salt mass on gamma-ray absorption, the following parameters were analyzed:

- The gross and net areas of the recorded spectrum.
- The gross and net areas of the background.
- The area of the photopeak and its net contribution.
- The full width at half maximum (FWHM) of the peak.
- The centroid position of the peak.
- The energy resolution (E.R%).

ISSN: 2312-8135 | Print ISSN: 1992-0652
info@journalofbabylon.com | jub@itnet.uobabylon.edu.iq | www.journalofbabylon.com

The experimental conditions were standardized with an applied voltage of 575 V, an amplifier gain of 2, and a counting time of 120 seconds.

Table (2): Effect of salt concentration on gamma-ray spectral parameters

Mass/200 ml (gm/cm^3)	Gross area	Net area	F.W.H.M	Centroid	E.R%
0	45643	43593	39	87	44.82759
5	41453	39 403	137	242	56.61157
10	36328	32911	102	244	41.80328
15	33589	32907	325	217	149.7696
20	33202	32861	227	199	114.0704

2.1 Effect of salt concentration on Gross Area

The relationship between the added salt mass and the gross area of the gamma-ray spectrum is illustrated in Figure (6). The data show a clear inverse relationship: as the salt concentration increases, the gross area decreases. This behavior is attributed to the enhanced absorptivity of the medium, as the dissolved salt increase the density of the solution , thereby attenuating more of the incident gamma radiation before it reaches the detector.

2.2 Effect of Salt Concentration on Net Area

Similarly, the variation of the net area with salt concentration is depicted in Figure (7). The results confirm that the net area decreases with increasing salt mass. This further supports the conclusion that the absorptivity of the solution increases with higher salt content, leading to reduced photon counts recorded by the detector.

2.3 Effect of Salt concentration on FWHM

The influence of salt concentration on the full width at half maximum (FWHM) of the energy spectrum is presented in Figure (8). The results demonstrate that the FWHM increases as the salt mass increases. This broadening of the peak indicates that the detector's resolution is affected by the increased density of the medium, which introduces additional scattering and absorption processes that degrade the sharpness of the photopeak.

2.4 Study of the Gamma-Ray Spectrum Regions

The effect of salt concentration on the centroid position of the photopeak and the corresponding energy resolution (E.R%) is shown in Figure (9). The results reveal that both the centroid position and the energy resolution vary significantly with the added salt mass. Specifically, the energy resolution increases with higher salt concentrations, reflecting the

ISSN: 2312-8135 | Print ISSN: 1992-0652
info@journalofbabylon.com | jub@itnet.uobabylon.edu.iq | www.journalofbabylon.com

deterioration of spectral clarity due to enhanced scattering and absorption. The observed broadening of the optical peak can be explained by the fact that the FWHM increases with the density of the medium. As the salt concentration rises, the NaI(Tl) scintillator becomes more sensitive to variations in photon interactions, leading to a proportional increase in both peak width and energy resolution.

2. 1 Effect (change in mass of salt added to 200 ml of pure water) on gross area

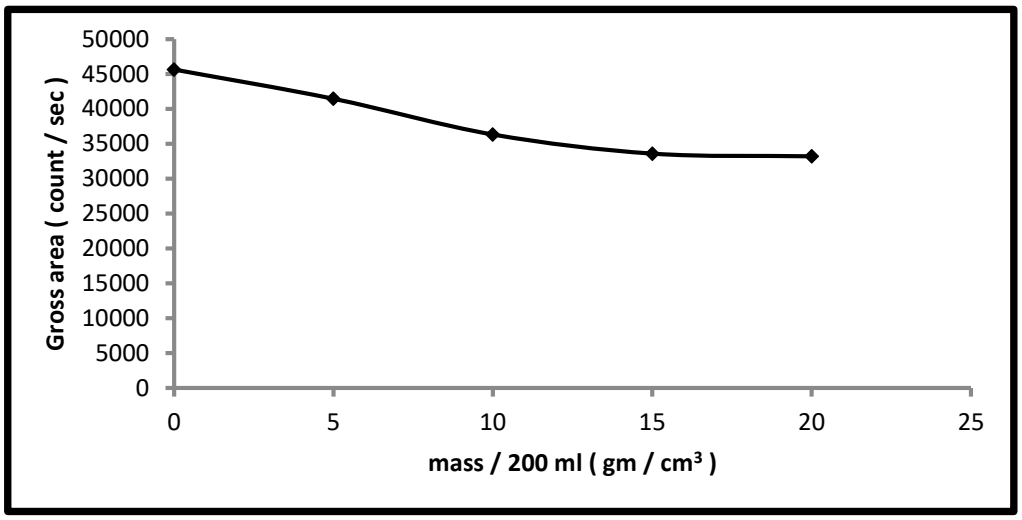

Figure (6): Shows the relationship between the change in mass of salt added to 200 ml of pure water and the gross area.

2.2 Effect of salt concentration change on net area of energy spectrum

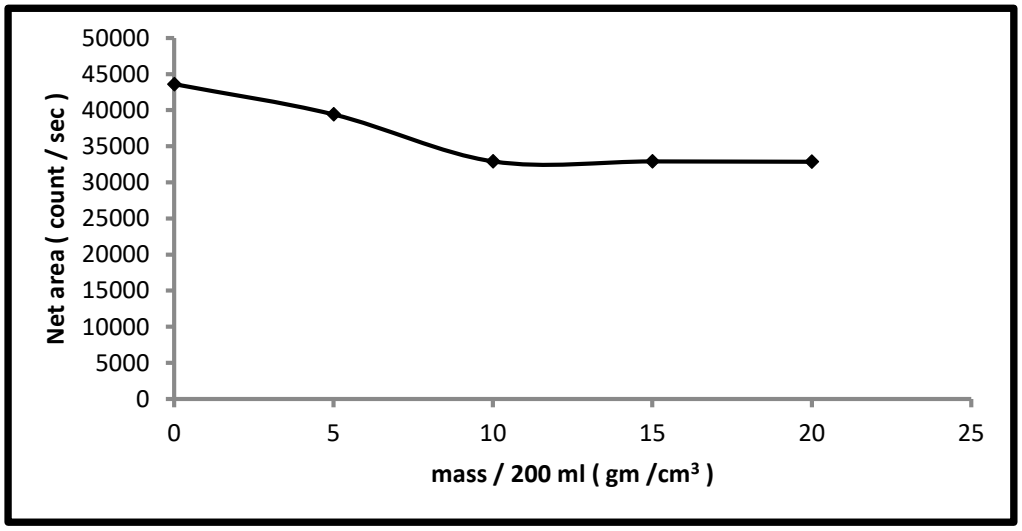

Figure (7): Shows the relationship between the change in salt mass added to 200 ml of pure water and the net area.

ISSN: 2312-8135 | Print ISSN: 1992-0652
info@journalofbabylon.com | jub@itnet.uobabylon.edu.iq | www.journalofbabylon.com

From the results in Table (2), Figures (6) and (7) were drawn between the added salt mass and the gross and net areas, respectively. It shows that the relationship between the mass of salt and the gross and net areas of the spectrum is inverse because the absorptivity of water for radiation passing through it increases with increasing salt concentration, which leads to a decrease in the two areas with increasing added mass.

2.3 Effect of salt mass change on the full width at half maximum (FWHM) of the energy spectrum.

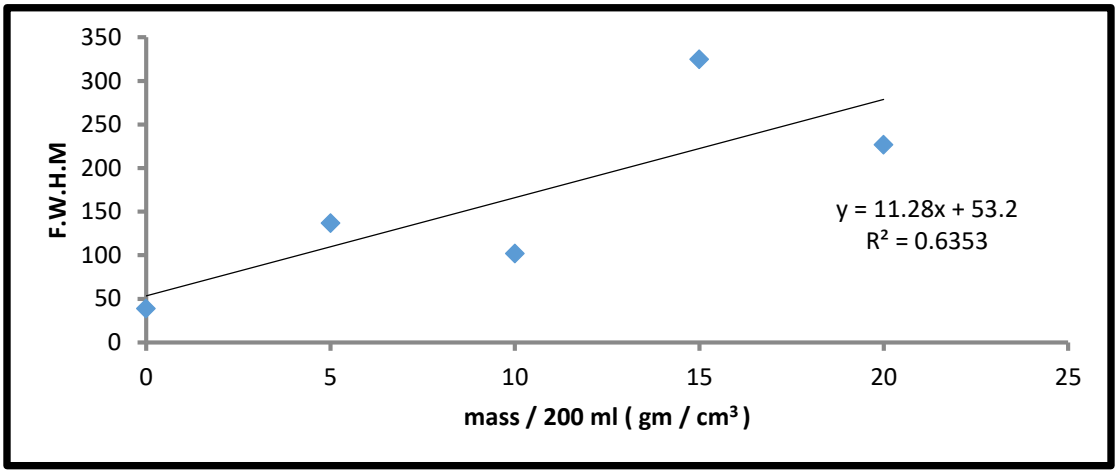

Figure (8): The relationship between the change in salt mass added to 200 ml of pure water and the full width at half maximum.

2.4. Effect of energy change on the center of the peak (CENTROID) and the energy resolution E.R %

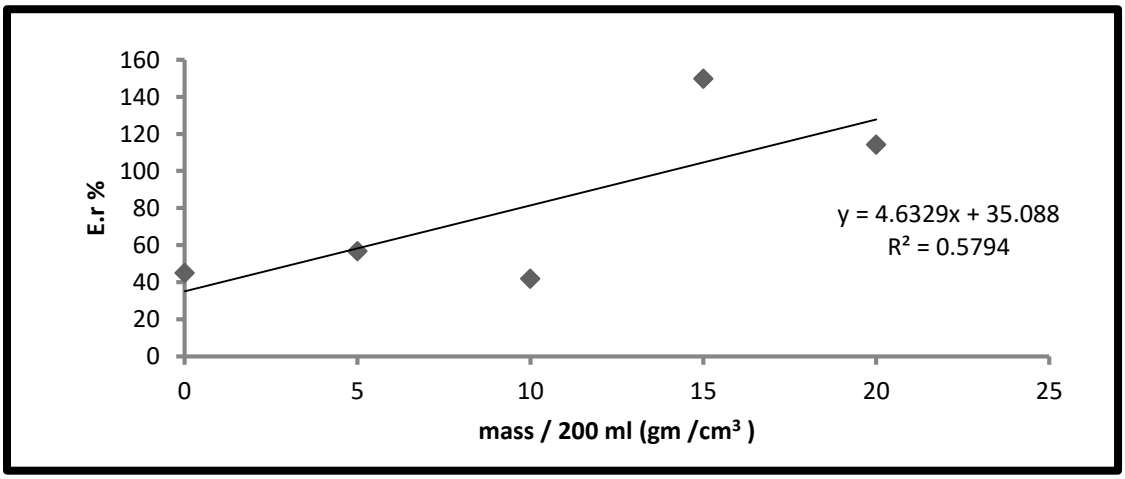

Figure (9): The relationship between the change in salt mass added to 200 ml of pure water and the energy resolution.

ISSN: 2312-8135 | Print ISSN: 1992-0652

info@journalofbabylon.com | jub@itnet.uobabylon.edu.iq | www.journalofbabylon.com

Based on the data presented in Table (2), Figures (8) and (9) illustrate the relationship between the mass of salt dissolved in 200 ml of water and two key spectral parameters: the full width at half maximum (FWHM) of the photopeak and the corresponding energy resolution (E.R%). The results clearly demonstrate a direct proportionality, where both the peak width and the energy resolution increase progressively with the addition of salt mass.

The observed broadening of the photopeak can be attributed to the increase in FWHM as the salt concentration rises. This effect is explained by the fact that the NaI(Tl) scintillation detector becomes increasingly influenced by the density of the medium through which the gamma radiation passes. As the density of the water–salt solution increases, the probability of photon scattering and partial energy deposition also increases, leading to a wider distribution of detected energies. Consequently, the detector exhibits a broader peak and a higher energy resolution value, both of which reflect the enhanced absorptivity and scattering effects introduced by the added salt.

CONCLUSION

The results showed that increasing the concentration of table salt in water leads to higher density and thus increases the medium's absorptivity of gamma rays emitted from the Cs-137 source, which reduces the number of photons recorded and leads to a broadening of the optical peak and a deterioration in spectral accuracy. This confirms that the composition of the surrounding medium directly affects the detector's response, which opens up prospects for applications in radiation protection, environmental monitoring and nuclear experiments.

Conflict of interests.

There are non-conflicts of interest.

References

[1] N. Channappa and B. R. Kerur, “Standardization of gamma-ray spectrometry using the NaI(Tl) scintillation detector,” *Journal of Radioanalytical and Nuclear Chemistry*, vol. 334, pp. 2171–2176, 2025.

[2] S. M. Kim and J. S. Lee, “A Comprehensive Review on Compton Camera Image Reconstruction: From Principles to AI Innovations,” *Biomedical Engineering Letters*, vol. 14, pp. 1175–1193, Sept. 2024.

[3] M. Niknami, S. A. Hosseini, and M. Valipour, “Compton Imaging Systems Based on CdZnTe/CdTe Detectors,” in *CdTe and CdZnTe Materials*, Springer, pp. 155–171, Aug. 2024.

[4] N. Tsoulfanidis and S. Landsberger, *Measurement and Detection of Radiation*, 4th ed., CRC Press, 2021.

[5] G. F. Knoll, *Radiation Detection and Measurement*, 4th ed., Wiley, 2010.

[6] D. Breitenmoser, M. Furrer, M. Hürlimann, A. Riedo, and R. Schmid, “Spectral gamma-ray response of NaI(Tl) detectors,” *Nucl. Instrum. Methods Phys. Res. A*, vol. 1025, pp. 166–222, 2022.

[7] M. A. Chowdhury, A. Bazza, A. El Hamli, M. Hamal, A. Moussa, M. Zerfaoui, L. Hamam, M. Ouchrif, and Y. Taylati, “NaI(Tl) Detector Response at Different Energies and a Validation with Monte Carlo Simulation,” in *Advances in Smart Technologies Applications and Case Studies (SmartICT 2019)*, Lecture Notes in Electrical Engineering, vol. 684, Springer, pp. 647–655, Aug. 2020.

[8] G. Pausch, A. Kreuels, F. Scherwinski, Y. Kong, M. Kuester, R. Lentering, A. Wolf, and J. Stein, "Fast- and thermal-neutron detection with common NaI(Tl) detectors using pulse-shape discrimination," *arXiv preprint* arXiv:2208.06696, Aug. 2022.
[9] A. Obertelli and H. Sagawa, *Modern Nuclear Physics: From Fundamentals to Frontiers*, Springer, 2021.
[10] R. Sh. Saiwan and J. M. Rashid, "Gradient shielding for scintillation detector NaI(Tl) using multiple materials," *Journal of College of Education for Pure Sciences*, Univ. of Thi-Qar, vol. 13, no. 2, pp. 45–53, 2023.
[11] International Atomic Energy Agency (IAEA), *Nuclear Technology Review 2023*, Vienna, 2023.
[12] J. Suhonen, *From Nucleons to Nucleus: Concepts of Microscopic Nuclear Theory*, Springer, 2021.
[13] J. Lilley, *Nuclear Physics: Principles and Applications*, 2nd ed., Wiley, 2022.
[14] M. J. Kumwenda, "A comparative study of unfolding techniques for gamma-ray spectra obtained with NaI(Tl) scintillation detectors," *Tanzania Journal of Science*, vol. 50, no. 2, pp. 994–1005, Dec. 2024.
[15] M. A. El-Taher, "Assessment of natural radioactivity levels and radiation hazards in soil samples from Egypt," *Journal of Environmental Radioactivity*, vol. 225, pp. 106–118, 2021.
[16] M. A. El-Taher and A. M. El-Khayatt, "Natural radioactivity levels and radiation hazard assessment in building materials using NaI(Tl) scintillation detector," *Radiat. Phys. Chem.*, vol. 180, p. 109271, 2021.
[17] M. A. El-Sersy, A. M. El-Khayatt, and H. M. Diab, "Measurement of depleted uranium concentrations in environmental samples using HPGe detectors," *Applied Radiation and Isotopes*, vol. 170, p. 109635, 2021.
[18] K. Heyde, *Basic Ideas and Concepts in Nuclear Physics: An Introductory Approach*, 4th ed., CRC Press, 2020.
[19] International Atomic Energy Agency (IAEA), *Nuclear Data Standards for Nuclear Measurements*, Technical Reports Series No. 488, Vienna, 2021.
[20] Y. Liu, X. Li, Y. Yin, Z. Li, H. Yao, and Z. Li, "Design and computational validation of γ-ray shielding effectiveness in heavy metal/rare earth oxide–natural rubber composites," *Polymers*, vol. 16, no. 15, p. 2130, July 2024.
[21] J. E. Martin, *Physics for Radiation Protection: A Handbook*, 3rd ed., Wiley, 2023.
[22] A. S. Tremsin, J. B. McPhate, and W. B. Feller, "High time resolution gamma-ray detection using fast scintillators and digital pulse-shape analysis," *IEEE Trans. Nucl. Sci.*, vol. 69, no. 5, pp. 1123–1131, May 2022.
[23] S. R. Cherry, J. A. Sorenson, and M. E. Phelps, *Physics in Nuclear Medicine*, 5th ed., Elsevier, 2022.

ISSN: 2312-8135 | Print ISSN: 1992-0652
info@journalofbabylon.com | jub@itnet.uobabylon.edu.iq | www.journalofbabylon.com

ISSN: 2312-8135 | Print ISSN: 1992-0652
info@journalofbabylon.com | jub@itnet.uobabylon.edu.iq | www.journalofbabylon.com

الخلاصة

بحثت هذه الدراسة تأثير تركيز ملح الطعام في الماء على امتصاص أشعة جاما المنبعثة من مصدر مشع للسيزيوم-137 .(Cs-137) أجريت القياسات باستخدام مطياف الكمبيوتر العالمي(UCS-30) ، الذي يمثل أحدث جيل من أنظمة التحليل الطيفي النووي التي طورتها شركةSpectrum Techniques LLC ، بعد الإصدارات السابقة مثل.UCS-20

أظهرت نتائج التجربة أن المساحة الإجمالية والمساحة الصافية لطيف طاقة أشعة جاما تنخفض تدريجياً مع زيادة تركيز الملح في حجم ثابت من الماء (200 مل). في المقابل، وجد أن مركز الذروة الضوئية والعرض الكامل عند نصف الحد الأقصى (FWHM) ودقة الطاقة تزداد مع زيادة تركيز الملح. تشير هذه النتائج إلى أن امتصاص الماء للأشعة جاما يتحسن بإضافة الملح، مما يؤدي إلى انخفاض عدد الفوتونات وتدهور دقة الطيف.

تسلط الدراسة الضوء على الدور المهم لكثافة المحلول في تعديل توهين أشعة جاما واستجابة الكاشف، مما يوفر رؤى مفيدة للتطبيقات في مجال الحماية من الإشعاع ومراقبة البيئة وتجارب الفيزياء النووية.

الكلمات المفتاحية: السيزيوم-137,(Cs-137) امتصاص أشعة غاما, كاشف وميضي ,NaI(Tl) تركيز ملح الطعام في الماء , الدقة الطاقية (عرض منتصف القمة)